THE JOURNAL OF BIOLOGICAL CHEMISTRY VOL. 286, NO. 8, pp. 6627–6640, February 25, 2011

Intraphagosomal Peroxynitrite as a Macrophage-derived Cytotoxin against Internalized *Trypanosoma cruzi*

CONSEQUENCES FOR OXIDATIVE KILLING AND ROLE OF MICROBIAL PEROXIREDOXINS IN INFECTIVITY[*] [S]

Received for publication, July 21, 2010, and in revised form, November 22, 2010 Published, JBC Papers in Press, November 23, 2010, DOI 10.1074/jbc.M110.167247

María Noel Alvarez, Gonzalo Peluffo, Lucía Piacenza, and Rafael Radi[1]

From the Departamento de Bioquímica and Center for Free Radical and Biomedical Research, Facultad de Medicina, Universidad de la República, Montevideo 11800, Uruguay

Macrophage-derived radicals generated by the NADPH oxidase complex and inducible nitric-oxide synthase (iNOS) participate in cytotoxic mechanisms against microorganisms. Nitric oxide ($^{\bullet}NO$) plays a central role in the control of acute infection by *Trypanosoma cruzi*, the causative agent of Chagas disease, and we have proposed that much of its action relies on macrophage-derived peroxynitrite ($ONOO^- + ONOOH$) formation, a strong oxidant arising from the reaction of $^{\bullet}NO$ with superoxide radical ($O_2^{\bullet-}$). Herein, we have shown that internalization of *T. cruzi* trypomastigotes by macrophages triggers the assembly of the NADPH oxidase complex to yield $O_2^{\bullet-}$ during a 60–90-min period. This does not interfere with IFN-γ-dependent iNOS induction and a sustained $^{\bullet}NO$ production (~24 h). The major mechanism for infection control via reactive species formation occurred when $^{\bullet}NO$ and $O_2^{\bullet-}$ were produced simultaneously, generating intraphagosomal peroxynitrite levels compatible with microbial killing. Moreover, biochemical and ultrastructural analysis confirmed cellular oxidative damage and morphological disruption in internalized parasites. Overexpression of cytosolic tryparedoxin peroxidase in *T. cruzi* neutralized macrophage-derived peroxynitrite-dependent cytotoxicity to parasites and favored the infection in an animal model. Collectively, the data provide, for the first time, direct support for the action of peroxynitrite as an intraphagosomal cytotoxin against pathogens and the premise that microbial peroxiredoxins facilitate infectivity via decomposition of macrophage-derived peroxynitrite.

Macrophages represent one of the first lines of defense against invading intracellular pathogens through their ability to recognize, ingest, and destroy microorganisms. The detection of infectious agents by pattern recognition receptors initiates signal transduction pathways, which leads to activation of the membrane-bound NADPH oxidase and induction of nitric-oxide synthase 2 (iNOS),[2] central components of oxidative-killing mechanisms. The NADPH oxidase complex is inactive in resting phagocytes and assembles upon stimulation, resulting in formation of antimicrobial superoxide radicals ($O_2^{\bullet-}$) within the phagosome (1, 2). The univalent reduction of oxygen by NADPH oxidase occurs immediately after phagocytosis, yielding high rates of $O_2^{\bullet-}$ for at least 90 min (3). Superoxide radical production can also result in the formation of H_2O_2 in the phagocytic vacuole either by spontaneous or extracellular SOD-catalyzed dismutation (4, 5). Macrophage cytotoxicity is enhanced by the presence of proinflammatory cytokines such as IFN-γ, which are secreted by natural killer cells (NK) in the first instance and by $CD4^+$ T helper-1 (Th1) cells once a specific immune response against the pathogen is established (6, 7). Following cytokine activation, macrophages produce large amounts of nitric oxide ($^{\bullet}NO$) because of induction of iNOS (8–10). In general terms, neither $O_2^{\bullet-}$ nor $^{\bullet}NO$ has been shown to be particularly cytotoxic *per se*, although the concomitant production of both radicals potentiates cytotoxicity (11–13).

We and others have proposed that the concerted actions of phagosomal NADPH oxidase and iNOS leads to the formation of peroxynitrite,[3] a potentially potent microbicidal species inside the phagosome (11, 12, 14–17). Because of its negative charge, the $O_2^{\bullet-}$ radical ($pK_a = 4.8$) remains within this organelle, whereas $^{\bullet}NO$, being a hydrophobic radical, diffuses from the cytosol or phagosomal membrane-associated iNOS (18) into the phagocytic vacuole. The reaction between $^{\bullet}NO$ and $O_2^{\bullet-}$ yields peroxynitrite (19, 20), a strong one- and two-electron oxidant and a precursor of secondary species including hydroxyl ($^{\bullet}OH$), nitrogen dioxide ($^{\bullet}NO_2$), and carbonate ($CO_3^{\bullet-}$) radicals (21). Peroxynitrite and peroxynitrite-derived radicals are capable of reacting with different biological targets including protein amino acid residues (*e.g.* thiol oxidation

* This work was supported by grants from the Howard Hughes Medical Institute and the International Centre for Genetic Engineering and Biotechnology (to R. R.), the Fondo Clemente Estable (Programa de Desarrollo Tecnológico) (to L. P.), and the Comisión Sectorial de Investigación Científica, Universidad de la República (to M. N. A.).

[S] The on-line version of this article (available at http://www.jbc.org) contains supplemental Figs. 1 and 2.

[1] A Howard Hughes International Research Scholar. To whom correspondence should be addressed: Dpto. de Bioquímica, Facultad de Medicina, Universidad de la República, Avda. General Flores 2125, Montevideo 11800, Uruguay. Tel.: 5982-9249561; Fax: 5982-9249563; E-mail: rradi@fmed.edu.uy.

[2] The abbreviations used are: iNOS, inducible nitric-oxide synthase; $^{\bullet}NO$, nitric oxide; $O_2^{\bullet-}$, superoxide radical; $^{\bullet}OH$, hydroxyl radical; $^{\bullet}NO_2$, nitrogen dioxide radical; $CO_3^{\bullet-}$, carbonate radical; DHR, dihydrorhodamine; NBT, nitro blue tetrazolium; DAF-2DA, 4,5-diaminofluorescein diacetate; DPI, diphenyliodonium; L-NMMA, N^G-monomethyl-L-arginine; *Tc*CPX, *T. cruzi* cytosolic tryparedoxin peroxidase; MPO, myeloperoxidase; DMPO, 5,5-dimethylpyrroline-*N*-oxide; SOD, superoxide dismutase; dPBS, Dulbecco's PBS; DIC, differential interference contrast; RH 123, rhodamine 123.

[3] The term peroxynitrite refers to the sum of peroxynitrite anion ($ONOO^-$) and peroxynitrous acid (ONOOH), $pK_a = 6.8$ (20, 21).

(22), tyrosine nitration (23)) transition metal-containing centers (24), lipids (25), and nucleic acids (26), reactions that can ultimately promote cell death by either apoptotic or necrotic pathways (27). The role of various oxidative mechanisms in the microbicidal activity of macrophages depends on a number of factors including, in the case of the oxidative mechanisms, a dynamic balance between the activation state of macrophages and the sensitivity of targets cells to oxidants (12, 28). However, the actual formation of peroxynitrite in the phagosome at levels that could be cytotoxic to invading microorganisms has remained elusive. Although in simple biochemical systems the reaction of $^{\bullet}NO$ with $O_2^{\bullet-}$ is very efficient, approaching the diffusion-controlled limit (21), in biological systems, competition reactions (*e.g.* SOD-catalyzed $O_2^{\bullet-}$ dismutation) (4), rapid diffusion of $^{\bullet}NO$ across biomembranes (29), and temporal mismatch between $^{\bullet}NO$ and $O_2^{\bullet-}$ production (30–32), among other factors, can preclude peroxynitrite formation. In addition, once formed, much of the peroxynitrite may be decomposed by reacting with noncritical targets and antioxidant enzymes (*i.e.* peroxiredoxins) (reviewed in Ref. 21), and therefore its potential cytotoxic effects are attenuated or even fully neutralized.

Trypanosoma cruzi is an obligate intracellular pathogen responsible for Chagas disease. It has been estimated that 8 million people are currently infected by the parasite, with 20% of Latin America's population (109 million) at risk resulting in 41,000 new cases each year (33). Moreover, the disease is spreading worldwide as a result of migration (mammalian hosts and insect vectors), HIV co-infection, blood transfusion, and organ transplantation. During its life cycle, *T. cruzi* undergoes extensive morphological and biochemical changes; non-infective epimastigotes proliferate in the gut of the insect vector where they differentiate into the infective metacyclic trypomastigotes. When initially infecting a host, the metacyclic form invades mainly host macrophages, where they can be destroyed by host immune mechanisms, including phagocytosis, or transformed into replicative intracellular amastigotes. After several cycles of binary division, host cell disruption occurs, and infective forms access the bloodstream and are able to invade cells from any tissue, such as the myocardium, smooth muscle, and central nervous system.

Biologically relevant levels of peroxynitrite are cytotoxic to non- infective epimastigote parasites (14). *In vitro* experiments have revealed that peroxynitrite addition to *T. cruzi* epimastigotes results in severe alterations of energy charge, calcium homeostasis, and depletion of trypanothione, the main low molecular weight thiol found in trypanosomatids (34). We have shown that macrophage-derived peroxynitrite has the capacity to diffuse and exert cytotoxicity against epimastigotes in co-culture experiments (13). Additionally, parasites overexpressing peroxiredoxins, antioxidant enzymes known to readily detoxify peroxynitrite (35, 36) and recently revealed as virulent factors in the human infection (37), are resistant to this reactive species (28). As early as 1974, the central role of macrophage phagocytosis in the control of *T. cruzi* infection was determined (38). Later, the importance of macrophages in *in vivo* infection was evidenced by experiments in which resistance to *T. cruzi* was associated with the production of IFN-γ and IL-12 in animal models (39, 40). Moreover, early treatment with IFN-γ was able to reverse the course of infection (41–43), presumably by controlling the early replication of parasites in host macrophages, with the participation of $^{\bullet}NO$ (44, 45).

Macrophage-derived $O_2^{\bullet-}$ production triggered by *T. cruzi* is a matter of debate, with discussion centered on the ability of trypomastigotes to activate NADPH oxidase (41, 46, 47). In regard to the modulation of $^{\bullet}NO$ production, contradictory results have been reported; although a negative regulation of iNOS induction by epimastigotes has been proposed (48, 49), experiments performed with trypomastigotes have shown potentiation of cytokine-mediated iNOS induction (50). Thus, the occurrence of $O_2^{\bullet-}$, $^{\bullet}NO$, and their reaction product, peroxynitrite, and how these reactive species participate independently or synergically in the ability of host macrophages to control *T. cruzi* infection require an unambiguous analysis. In this work, we first studied whether *T. cruzi* infection of activated macrophages results in the simultaneous production of $^{\bullet}NO$ and $O_2^{\bullet-}$ and leads to the intraphagosomal formation of peroxynitrite. We then evaluated the capacity of peroxynitrite *versus* that of $^{\bullet}NO$ and $O_2^{\bullet-}$ (and H_2O_2) alone to efficiently serve as cytotoxins to control the load of internalized parasites. Finally, we tested the role of the cytosolic parasite peroxiredoxin in neutralizing the effects of host cell-derived oxidants *in vitro* and *in vivo* with the possible consequent promotion of infectivity. The data presented herein assist in understanding the mechanisms of oxidant-dependent killing of internalized pathogens.

EXPERIMENTAL PROCEDURES

Reagents

Murine recombinant IFN-γ, human myeloperoxidase (MPO), and the anti-human MPO antibody were purchased from Calbiochem. Dulbecco's modified Eagle's medium (DMEM), lipopolysaccharide (LPS), luminol, N^G-monomethyl-L-arginine (L-NMMA), apocynin, [5,6-^{3}H]uridine (30 Ci mmol^{-1}), Geneticin (G418), nitro blue tetrazolium (NBT), diphenyliodonium (DPI), and the anti-N-terminal region of actin antibody were from Sigma. Lab-Tek tissue culture chamber slides were from Nunc. 4′-6-Diamidino-2-phenylindole (DAPI), dihydrorhodamine (DHR), and Alexa-Fluor 488- and 594-conjugated anti-rabbit antibodies were from Invitrogen. 4,5-Diaminofluorescein diacetate was from Alexis Biochemicals. All other reagents were of research grade quality.

Parasite Culture and Differentiation

T. cruzi epimastigotes (CL-Brener) were cultured at 28 °C in brain-heart infusion medium as described previously (51). Parasites overexpressing cytosolic tryparedoxin peroxidase (*Tc*CPX) were kindly provided by Dr. Shane Wilkinson (Queen Mary University of London, United Kingdom) (52) and were cultured in brain-heart infusion medium containing 250 μg ml^{-1} G418 (Sigma) (28). Parasites were differentiated into the infective metacyclic stage under chemically defined conditions as described previously (53). Briefly, epimastigotes were collected by centrifugation at 800 × *g* for 10 min at 25 °C, washed three times in 10 ml of triatomine artificial

urine medium (TAU: 190 mM NaCl, 17 mM KCl, 2 mM $MgCl_2$, 2 mM $CaCl_2$, 8 mM phosphate, pH 6, and 0.035% sodium bicarbonate), and resuspended at a cell density of 3–5 $\times$ 10^8 cells ml^{-1}. After 2 h of incubation at 28 °C, parasites were diluted in TAU-3AAG medium (TAU, pH 6, supplemented with three amino acids: 10 mM L-proline, 50 mM sodium L-glutamate, 2 mM sodium L-aspartate, and 10 mM glucose) at 3–5 $\times$ 10^6 cells ml^{-1}. Cells were incubated for 96 h at 28 °C in 75-cm^2 culture flasks in a horizontal position to allow adhesion of epimastigotes to the flask surface, an important step in enabling parasites to be transformed into the infective metacyclic trypomastigote stage (54).

Macrophages Culture

The murine macrophage cell line J774A.1 (American Type Culture Collection (ATCC-TIB-67)) was cultured in DMEM (Sigma) supplemented with L-glutamine (2 mM), penicillin (100 units ml^{-1}), streptomycin (100 mg l^{-1}), and 10% heat-inactivated fetal bovine serum at 37 °C in a 5% CO_2 atmosphere.

Macrophage $O_2^{\cdot-}$ Production

Luminol Chemiluminescence—Macrophages were cultured in 24-well plates, and $O_2^{\cdot-}$ production was assayed by chemiluminescence studies as described previously (13). Briefly, macrophages were incubated under different experimental conditions in Dulbecco's PBS (dPBS), pH 7.3, containing 5 mM glucose, 1 mM L-arginine, and 100 μM luminol; the time course of luminol chemiluminescence was followed for 100 min in a luminescence plate reader at 37 °C (Lumistar, BMG Labtechnologies).

Intracellular Detection of Reduced NBT—Macrophages were seeded in Lab-Tek tissue culture chamber slides (Nunc) and infected with *T. cruzi* metacyclic trypomastigotes (5:1, parasite:macrophage ratio) in dPBS containing 1 mg/ml NBT (55). Slides were incubated at 37 °C for 30 min, rinsed in warmed dPBS, fixed for 10 min in 4% (v/v) formaldehyde in PBS at room temperature, and stained with DAPI (5 μg ml^{-1}). Cells that contained formazan-stained inclusions within phagocytic vacuoles were observed by differential interference contrast (DIC) microscopy, and internalized trypomastigotes were evidenced by colocalization of the formazan deposits with DAPI fluorescence.

Oxygen Consumption by Macrophages—Macrophage mitochondrial respiration and respiratory burst were evaluated using a high resolution electrode, Oxygraph 2K (Oroboros Instruments, Innsbruck, Austria). Cells were cultured in 6-well plates and challenged with opsonised zymosan (56) or *T. cruzi* metacyclic trypomastigotes in DMEM. Interaction was synchronized by plate centrifugation (800 $\times$ *g*, 5 min), and following a 15-min incubation at 37 °C non-internalized zymosan or parasites were removed. Macrophages were resuspended at 1 $\times$ 10^6 cells/ml in DMEM, and O_2 consumption was recorded at 37 °C. The rate of oxygen consumption was calculated using DatLab 4.3 software (Oroboros Instruments) and was expressed as nmol O_2 $min^{-1}/10^6$ cells. Oxygen consumption inhibited by 1 mM potassium cyanide corresponds to mitochondrial respiration. The cyanide-insensitive fraction was inhibited by 100 μM DPI and corresponds to NADPH oxidase activity (57).

Macrophage $^{\cdot}$NO Production

The induction of the macrophage iNOS was triggered by incubating the cells with 200–300 units ml^{-1} IFN-γ (Calbiochem) plus 3 μg ml^{-1} LPS (Sigma) for 5 h (3). $^{\cdot}$NO production by unstimulated or IFN-γ/LPS-activated macrophages was evaluated in tissue culture. Cells were seeded at 1 $\times$ 10^6 cells/well in the presence or absence of *T. cruzi* epimastigotes or chemically differentiated metacyclic trypomastigotes (see above). Following incubation (for 24 h), supernatants were collected, and the concentration of nitrite (NO_2^-) was determined spectrophotometrically at 540 nm using the Griess method with $NaNO_2$ as the standard (3, 58). Macrophage-$^{\cdot}$NO production was also evaluated using the cell-permeable fluorescence probe 4,5-diaminofluorescein diacetate (DAF-2DA) (59). After 5 h of incubation with the iNOS inducers, the medium was replaced with dPBS with 5 mM glucose and 1 mM L-arginine containing 5 μM DAF-2DA. Probe oxidation was followed in a fluorescence plate reader at 37 °C (Fluostar, BMG Labtechnologies) with filters at λ_{ex} = 485 nm and λ_{em} = 520 nm. Under our experimental conditions, the peroxynitrite-dependent reactions (60) did not interfere with the fluorophore.

Measurements of iNOS Messenger RNA Levels

Macrophages were seeded in 6-well plates (5 $\times$ 10^6 cells/well) and infected at a 10:1 parasite:macrophage ratio. After 3 h of infection total RNA was extracted using the PureLink™ Micro-to-Midi™ Total RNA purification system (Invitrogen), and a cDNA copy was obtained using the SuperScript™ III first-strand system for RT-PCR (Invitrogen). iNOS mRNA in each condition was amplified using the primers 5′-CTAAGAGTCACCAAAATGGCTCCC-3′ and 5′-ACCAGAGGCAGCACATCAAAGC-3′, which yielded an 875-bp band of murine iNOS. The housekeeping gene glyceraldehyde-3-phosphate dehydrogenase (*GAPDH*) was amplified to verify equal cDNA loading in each condition with the primers 5′-CTGAGAACGGGAAGCTTGTC-3′ and 5′-CCTGCTTCACCACCTTCTTG-3′, which yielded a 600-bp band. Polymerase chain reaction was carried out using 5 μg of cDNA at an annealing temperature of 58 °C. PCR products were resolved by electrophoresis in 2% agarose gel, fragments were visualized with ethidium bromide, and gels were registered with a digital Polaroid camera.

Immunochemical Evaluation of Myeloperoxidase

Mice neutrophils, used as a positive control for MPO detection, were purified from peripheral blood as described (61). For protein extraction, neutrophils and J774A-1 macrophages were lysed in radioimmune precipitation assay buffer (150 mM NaCl, 10 mM Na_2HPO_4, pH 7.2, 0.1% SDS, 1% Triton X-100, and 1% sodium deoxycholate) supplemented with a mixture of protease inhibitors (Sigma). For immunoblotting, samples were separated by SDS-PAGE (10%) and transferred onto a PVDF membrane (Millipore). The membrane was incubated with a rabbit poly-

clonal anti-human MPO antibody (Calbiochem) and horseradish peroxidase-conjugated antibody as the secondary antibody. The blots were developed with ECL reagent (Amersham Biosciences). The nitrocellulose membrane was stripped and reblotted with anti-actin antibody (Sigma).

Intracellular Dihydrorhodamine Oxidation

Metacyclic trypomastigotes were incubated for 20 min in dPBS, pH 7.4, containing 50 μM DHR for intracellular probe incorporation and washed twice in dPBS before the assay. Macrophages were infected with DHR-loaded metacyclic trypomastigotes for 30 min at 37 °C and washed in dPBS to remove non-internalized parasites. Intracellular rhodamine 123 (RH 123, oxidation product of DHR) formation under the different macrophage stimulation conditions was measured in a fluorescence plate reader at 37 °C (Fluostar, BMG Labtechnologies) with filters at $\lambda_{ex} = 485$ nm and $\lambda_{em} = 520$ nm (3). To evaluate rhodamine localization, cells were examined by fluorescence microscopy, and digital photographs of infected macrophages were recorded.

Immunocytochemistry Studies

Macrophages cultured in Lab-Tek glass chamber slides were exposed to different conditions and then fixed in 4% formaldehyde at room temperature for 5 min. They were then rinsed in PBS and permeabilized with 0.1% Triton X-100 in PBS prior to primary antibody exposition.

Immunodetection of iNOS expression was performed using a rabbit anti-iNOS (1:100) (Sigma). After copious washes, the slides were then incubated for 1 h with a secondary goat anti-rabbit antibody conjugated to Alexa Fluor 594 (Invitrogen) diluted 1:500 in 0.005% (v/v) Triton X-100 in PBS.

Immunodetection of 5,5-dimethylpyrroline-*N*-oxide (DMPO)-nitrone protein adducts on internalized parasites was performed using a rabbit anti-DMPO-nitrone serum that binds to the one-electron oxidation product of the initial DMPO nitroxyl protein spin adduct (62). Parasites were incubated with DMPO (100 mM) in dPBS for 30 min at 28 °C. After incubation, parasites were collected by centrifugation at 800 × *g* for 10 min at 25 °C and used in infection assays in Lab-Tek tissue culture chamber slides. Following macrophage infection (2 h) with preloaded trypomastigotes, cells fixed and permeabilized as described above were incubated for 30 min in a blocking solution containing 1% BSA in PBS, pH 7.4. Slides were then incubated for 1 h with the polyclonal anti-DMPO-nitrone (1:100). After three washes in 0.01% (v/v) Triton X-100 in PBS, secondary goat anti-rabbit antibody conjugated to Alexa Fluor 594 (Invitrogen) and diluted 1:500 in 0.005% (v/v) Triton X-100 in PBS was added for 1 h. Nuclei were visualized with DAPI (5 μg ml^{-1}).

For protein 3-nitrotyrosine immunodetection, fixed cells were blocked and incubated with rabbit anti-3-nitrotyrosine antisera produced in our laboratory (1:100) (63) and, thereafter, with a goat anti-rabbit IgG antibody labeled with Alexa Fluor 488 (1:500). All slides were examined using an epifluorescence microscope.

Transmission Electron Microscopy

Infected macrophages were also prepared for examination by transmission electron microscopy. After the indicated incubation periods, the cells were fixed with a solution containing 4% (w/v) paraformaldehyde/0.2% (w/v) glutaraldehyde in PBS, pH 7.4, rinsed in the same buffer, and then post-fixed in 1% osmium tetroxide, dehydrated through graded ethanol solutions, and embedded in Araldite resin. Sections were made on an RMC MT-X Ultramicrotome with a DiATOME diamond knife. Ultrathin sections (40–60 nm) were stained with uranyl acetate and lead citrate and examined with a JEOL JEM-1010 electron microscope operating at 80 kV. The images were obtained with a Hamamatsu C-4742-95 digital camera and processed with the Photoimpact program.

T. cruzi Cytotoxicity Assay

T. cruzi metacyclic trypomastigotes were incubated for 24 h in 10 μCi ml^{-1} [5,6-^{3}H]uridine at 28 °C. After incubation, the labeled parasites were collected by centrifugation at 800 × *g* and washed three times in dPBS, pH 7.4, to eliminate non-incorporated [5,6-^{3}H]uridine. Macrophages were infected for 30 min at 37 °C with [5,6-^{3}H]uridine-loaded metacyclic trypomastigotes (parasite:macrophage ratio of 5:1). Infection was synchronized by plate centrifugation (800 × *g*, 5 min), and following a 30-min incubation at 37 °C, cell supernatant containing non-internalized parasites (S1) was removed and conserved for quantification of the total count present in each condition. Macrophages were then washed three times with dPBS, pH 7.4, and after a 2-h incubation in DMEM at 37 °C, supernatants were collected (S2, killed parasites). Pelleted, infected macrophages were lysed in 200 μl of TET buffer (10 mM Tris/HCl, 1 mM EDTA, pH 8, with 0,5% Triton X-100). Cell pellets (P) and supernatants (S1 and S2) were each mixed with 3 ml of scintillation fluid, and radioactivity was measured in a liquid scintillation counter (Trilux 1450 Microbeta, Wallac Instruments). The results are expressed as a percentage of [5,6-^{3}H]Uridine released during the 2-h infection period (S2) with respect to total [5,6-^{3}H]uridine incorporation (p + S1 + S2) for each condition and represent the mean of three independent experiments.

Determination of Parasite Load in Macrophages

Macrophages were seeded in Lab-Tek tissue culture chamber slides and incubated for 5 h with or without iNOS inducers (IFN-γ plus LPS) before infection with metacyclic trypomastigotes (parasite:macrophage ratio of 5:1) for 1 h at 37 °C. Non-engulfed parasites were removed by washing twice in dPBS, and macrophages were further incubated for 24 h in DMEM at 37 °C. Infected macrophages were fixed in a 4% (v/v) formaldehyde solution in PBS for 10 min at room temperature, washed with PBS containing 100 mM glycine, and permeabilized for 5 min with 0.1% (v/v) Triton X-100 in PBS. The number of parasites per macrophage was determined by DAPI staining (5 μg ml^{-1}). Preparations were analyzed using a microscope (Nikon Eclipse TE-200 inverted microscope) at ×1000 magnification, and digital photographs of infected macrophages were recorded. At least 2500 cells from five independent experiments were counted. Results are expressed

as the number of amastigotes/100 macrophages under each condition and represent the mean of five independent experiments.

Parasitemia and Histopathological Analysis

BALB/c mice ($n = 6$) were infected with 1×10^6 metacyclic trypomastigotes by intraperitoneal injection with wild type parasites or *T. cruzi* overexpressing *Tc*CPX. The blood (10 μl) of anesthetized mice was used to determine the parasite load and the number of trypomastigotes/100 fields of view every 10 days. After 60 days, tissue samples (heart and quadriceps muscle) of infected mice were recovered and fixed in 10% (v/v) fresh formaldehyde. Paraffin-embedded tissue sections (four nonconsecutive slides) from the heart and quadricep muscles of each mouse were stained with hematoxylin-eosin and examined under a light microscope (64).

Microscopy Analysis

Imaging was performed using a Nikon Eclipse TE-200 inverted microscope coupled to a camera (SPOT RT camera, Diagnostic Instruments Inc.). Images were analyzed using ImageJ, a public domain Java image-processing program.

Data Analysis

Experiments were performed at least three times on independent days. All data are given as mean ± S.D. unless otherwise noted, and $p < 0.05$ was considered significant. Means were compared using the Student's *t* test. For comparison of more than two groups, an analysis of variance and a least-significant-difference post hoc test were performed.

RESULTS

T. cruzi Trypomastigotes Trigger $O_2^{\cdot-}$ Production by Macrophage NADPH Oxidase—We examined the capacity of *T. cruzi* trypomastigotes to trigger $O_2^{\cdot-}$ production by activation of NADPH oxidase during phagocytosis. The respiratory burst at the phagosome level was evaluated using a qualitative assay in which NBT is converted into a dark formazan precipitate following its reduction by $O_2^{\cdot-}$; this can be visualized by microscopy (Fig. 1*A*, *NBT*). Unstimulated macrophages were infected with trypomastigotes (parasite:macrophage ratio, 5:1) for 30 min and examined using DIC microscopy. Fig. 1 shows the precipitated dark formazan inside the phagosome (indicated by *arrows*), which co-localized with DAPI-stained trypomastigote nuclei inside the vacuole (Fig. 1*A*, *DAPI*). This indicates that $O_2^{\cdot-}$ formation is occurring on the luminal side of the phagosome. The formation of formazan upon *T. cruzi* invasion was completely abolished by pretreatment of macrophages with the NADPH oxidase inhibitor apocynin (Fig. 1*A*), a compound that prevents $p47^{PHOX}$ subunit translocation and therefore assembly of the enzyme complex. Moreover, NBT reduction was also prevented by the flavoprotein inhibitor DPI (50 μM) and by SOD (2 μM; not shown), fully confirming that the parasite-generated respiratory burst is dependent on NADPH oxidase-derived $O_2^{\cdot-}$.

To further characterize $O_2^{\cdot-}$ production by macrophages, we conducted chemiluminescence experiments using luminol, which can serve as a probe for $O_2^{\cdot-}$ and/or peroxynitrite (20, 65) and allows evaluation of the steady state levels reached by these oxidants. Time course experiments in unstimulated macrophages showed an $O_2^{\cdot-}$ production for ~60–90 min, which peaked after 10 min of infection (Fig. 1*B*, *inset*). Superoxide production triggered by the infective trypomastigote was 5-fold higher than that observed with the non-infective epimastigote and was dependent on the number of parasites used to infect macrophages (Fig. 1*B*). Luminol chemiluminescence was almost fully abolished by apocynin (Fig. 1*B*, *apo*) and SOD (not shown; see also Ref. 13). Peroxynitrite did not contribute to chemiluminescence in unstimulated macrophages, as light emission did not decrease by pretreatment of the cells with the iNOS inhibitor L-NMMA (not shown), consistent with their lack of significant iNOS activity (see Fig. 2). Interestingly, a higher chemiluminescence signal was observed upon *T. cruzi* invasion of macrophages that had been prestimulated for $^{\cdot}NO$ formation (Fig. 1*B*, *inset*). In this case, light emission was inhibited by L-NMMA (Fig. 1*B*), reaching levels comparable with those observed in unstimulated macrophages and fully supporting the formation of peroxynitrite, an efficient inducer of luminol chemiluminescence (66).

To quantitate $O_2^{\cdot-}$ production by trypomastigote-challenged macrophages, we determined the cyanide-insensitive and DPI-inhibitable oxygen consumption, which corresponds to the respiratory burst. Macrophages challenged with *T. cruzi* caused an increase in oxygen consumption rates, the extent of which was dependent on the number of parasites (0.72 ± 0.08 and 1.19 ± 0.37 nmol/min/10^6 macrophages for *T. cruzi*/macrophage ratios of 2:1 and 5:1, respectively). These data on NADPH activity obtained from macrophages during *T. cruzi* invasion were within the order of magnitude observed during phagocytosis of opsonized-zymosan particles (data not shown and Ref. 67), the standard method for respiratory burst evaluation.

Differential Modulation of Macrophage $^{\cdot}NO$ Production by Epimastigotes and Trypomastigotes—Experiments were conducted to explore the effect of trypomastigotes on the $^{\cdot}NO$ output and iNOS mRNA level in macrophages. Exposure of the mammalian cells to infective *T. cruzi* before activation by INF-γ and LPS did not affect the accumulation of nitrite, measured as an index of $^{\cdot}NO$ formation, at 24 h (Fig. 2*A*). In contrast, non-infectious epimastigotes caused an inhibition on $^{\cdot}NO$ production by iNOS that was dependent on the number of parasites interacting with macrophages (Fig. 2*A*). The rates of $^{\cdot}NO$ production were evaluated by the L-NMMA-inhibitable DAF-2DA oxidation, an intracellular fluorescence probe for $^{\cdot}NO$ (59). Again, although the presence of trypomastigotes did not affect macrophage iNOS activity, epimastigotes strongly inhibited $^{\cdot}NO$ formation (Fig. 2*B*).

Further, we also explored the effect of trypomastigotes on macrophage iNOS mRNA levels. As shown on Fig. 2*C*, trypomastigotes did not affect mRNA levels after the induction of iNOS by INF-γ and LPS (*lane 3*). Moreover, in the presence of INF-γ alone, trypomastigotes caused some further increase of mRNA levels for iNOS (Fig. 2*C*, *lane 5*); the relevance of this observation was confirmed by an increase in DAF-2DA oxidation when using macrophages activated by INF-γ in the

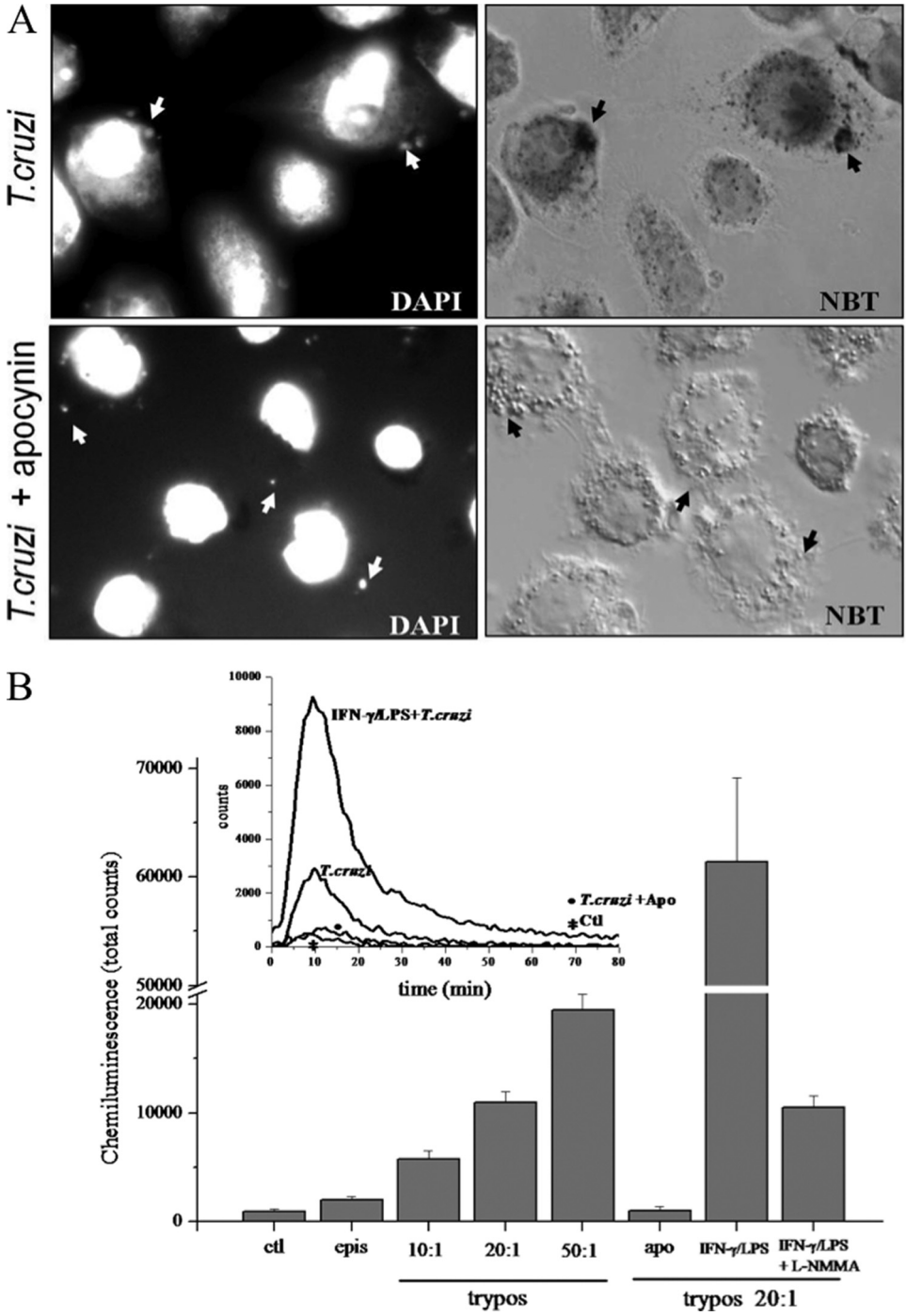

FIGURE 1. **Phagocytosis of *T. cruzi* trypomastigotes is accompanied by intraphagosomal- and NADPH oxidase-dependent $O_2^{\cdot-}$ formation.** *A*, superoxide-dependent intraphagosomal NBT reduction. Macrophages were incubated with *T. cruzi* trypomastigotes (5:1 ratio) in the presence of NBT (1 mg/ml, 30 min, 37 °C) and apocynin (50 μM) as indicated, stained with DAPI as described under "Experimental Procedures," and observed by fluorescence/Nomarski DIC microscopy (magnification, ×1000). *Arrows* indicate internalized parasites visualized by DAPI-stained nuclei (*upper* and *lower left*) within phagosomes as evidenced by formazan deposits (*upper right*). Apocynin completely abolished $O_2^{\cdot-}$-dependent formazan formation (*lower right*). Data shown are representative of at least three independent experiments performed on separate days. *B*, luminol chemiluminescence. Macrophages (1×10^6) incubated in dPBS with 200 μM luminol were exposed to: *T. cruzi* epimastigotes (2×10^7) and trypomastigotes (1, 2, and 5×10^7) corresponding to a trypomastigotes:macrophage ratio of 10:1, 20:1, and 50:1. The effect on luminol chemiluminescence of apocynin (*apo*), iNOS induction (*IFN-γ/LPS*), and inhibition by L-NMMA (*IFN-γ/LPS + L-NMMA*) was explored at a 20:1 ratio. Chemiluminescence was continuously measured immediately after *T. cruzi* addition to the macrophage monolayer in a luminescence plate reader at 37 °C. Data represent mean ± S.E. of total counts in 100 min. *Inset*, shows representative records obtained by the addition of trypomastigotes (20:1) to unstimulated (*T. cruzi*), apocynin-treated (*T. cruzi + Apo*), or preactivated macrophages (*IFN-γ/LPS + T. cruzi*). *ctl*, control (correspond to macrophages not challenged with *T. cruzi*.); *epis*, epimastigotes; *trypos*, trypomastigotes.

presence of trypomastigotes *versus* INF-γ-activated macrophages alone (data not shown). Finally, although iNOS induction by INF-γ plus LPS was inhibited by epimastigotes, full protein expression was obtained in the presence of trypomastigotes (Fig. 2*D*), consistent with the data obtained for •NO production and iNOS mRNA levels.

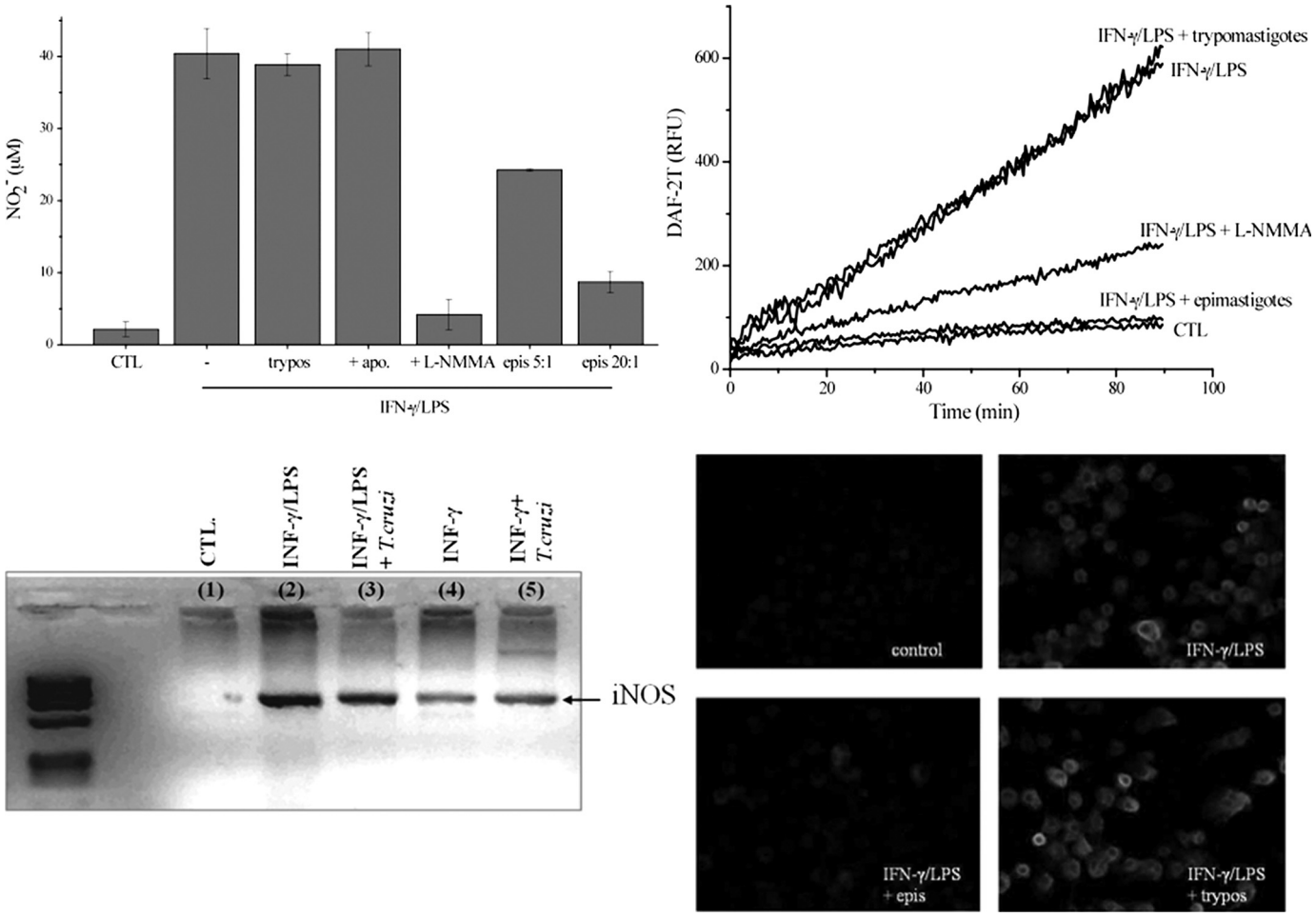

FIGURE 2. **Nitric oxide production and iNOS levels in *T. cruzi*-infected macrophages.** *A*, nitrite production. Macrophages were exposed to IFN-γ/LPS for 24 h in the absence and presence of epimastigotes (epimastigotes:macrophages, 5:1 and 20:1) or trypomastigotes (20:1). The effect of apocynin (*apo*) and L-NMMA (2 mM) was also evaluated. Nitrite accumulation was determined using the Griess reaction. *epis*, epimastigotes; *CTL*, control; *trypos*, trypomastigotes. *B*, DAF-2DA oxidation. Macrophages were exposed to IFN-γ/LPS in the presence of epimastigotes (20:1), trypomastigotes (20:1), or L-NMMA (2 mM) in DMEM at 37 °C. Control experiments were performed in the absence of cytokine stimulation. After 5 h, the medium was replaced with dPBS containing 5 μM DAF-2DA, and probe oxidation was followed in a fluorescence plate reader at 37 °C. *RFU*, relative fluorescence units. *C*, iNOS mRNA levels of macrophages exposed to IFN-γ/LPS, IFN-γ/LPS + trypomastigotes (10:1), IFN-γ, and IFN-γ + trypomastigotes (10:1) were evaluated by RT-PCR. Total RNA from 5×10^6 macrophages under all conditions was extracted after 3 h of infection. Host iNOS and GAPDH cDNAs were amplified using primers defined under "Experimental Procedures." *D*, iNOS expression was evaluated by immunocytochemistry. Macrophages plated in slides were stimulated for 5 h with IFN-γ/LPS in the presence or absence of *T. cruzi* epimastigotes or trypomastigotes. Immunocytochemical analysis of iNOS expression was performed using polyclonal anti-NOS antibody and visualized with Alexa-594-conjugated anti-rabbit antibody (magnification, ×400). Data shown are representative of at least three independent experiments performed on separate days.

Phagocytosed T. cruzi Trypomastigotes Are Targets of Intraphagosomal Peroxynitrite—The concomitant formation of $O_2^{\cdot-}$ and $^{\cdot}NO$ during infection by trypomastigotes is expected to yield peroxynitrite, as these two free radicals react with each other at diffusion control rates ($k \sim 10^{10}$ M^{-1} s^{-1}). Once formed, peroxynitrite could diffuse to and react with molecular targets in the parasite directly or through formation of secondary radicals such as $^{\cdot}OH$, $^{\cdot}NO_2$, and $CO_3^{\cdot-}$ (13). To evaluate whether peroxynitrite reaches the cytosol of phagocytosed cells, trypomastigotes preloaded with the redox-sensitive probe DHR were used to infect macrophages. DHR can be oxidized to the fluorescent RH 123 by a group of strong oxidants (68); thus, appropriate control experiments are required to assist in revealing the nature of the main proximal reactive species responsible of its oxidation. Indeed, peroxynitrite-derived radicals efficiently oxidize DHR, which can be monitored by fluorescence spectroscopy and microscopy (20). In fact, during phagocytosis maximal DHR oxidation yields were obtained in macrophages activated previously with IFNγ/LPS, where the simultaneous formation of $^{\cdot}NO$ and $O_2^{\cdot-}$ is present, indicating peroxynitrite formation during the infection process (Fig. 3*A*). Under experimental conditions in which macrophages were stimulated to produce exclusively $O_2^{\cdot-}/H_2O_2$ (*i.e.* unstimulated macrophages) or $^{\cdot}NO$ (*i.e.* IFNγ/LPS-activation plus apocynin), no significant DHR oxidation was detected (Fig. 3*A*). DHR oxidation in IFNγ/LPS-stimulated cells was also largely inhibited by iNOS inhibitors (not shown) as reported previously (3). When infected IFNγ/LPS-activated macrophages were observed by fluorescence microscopy, fluorescent RH 123 was found at locations compatible with phagocytosed trypomastigotes (Fig. 3*B*). Finally, to further confirm that peroxynitrite was formed in the phagosome, we examined protein oxidative modifications such as formation of protein-derived radicals and nitration of tyrosine resi-

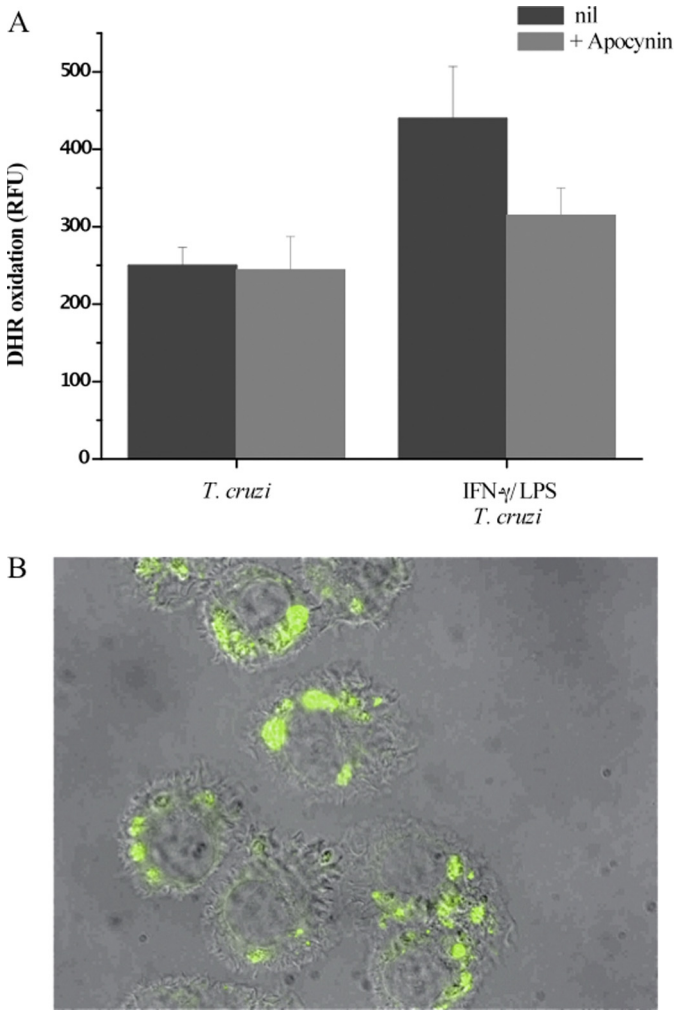

FIGURE 3. **DHR oxidation inside phagocytosed trypomastigotes.** *T. cruzi* trypomastigotes preloaded with DHR were exposed to macrophages, and cells were washed 30 min after incubation. *A*, RH 123 accumulation after 2 h of infection in unstimulated (*T. cruzi*) or preactivated macrophages (IFN-γ/ LPS + *T. cruzi*) was determined in a fluorescence plate reader. The effect of apocynin was evaluated under both conditions (+ *Apocynin*). *RFU*, relative fluorescence units. Data are mean ± S.E. of three independent experiments. *B*, activated macrophages plated in slides were infected with DHR-loaded trypomastigotes (5:1, parasite:macrophage ratio). Merged DIC and fluorescence images were obtained 2 h after infection; the *green* fluorescence corresponds to oxidized DHR (magnification, ×400).

dues, which could be attributed to radicals derived from peroxynitrite. Oxidative modifications of proteins were evidenced by immunocytochemical analysis (*a*) by immunospintrapping using an anti-DMPO-nitrone antibody (69) and (*b*) with anti-3-nitrotyrosine antibodies (63). Infected IFN-γ/ LPS-activated macrophages had positive immunostaining for both DMPO-nitrone (Fig. 4*A*) and 3-nitrotyrosine (Fig. 4*B*) adducts. The punctuate pattern observed in the infected cells demonstrates that these protein modifications occur in the internalized trypomastigotes, as they are localized in close proximity to the *T. cruzi* nuclei and kinetoplasts (Fig. 4), fully supporting oxidative damage to parasite proteins inside the phagosome.

Importantly, considering that $O_2^{\cdot-}$ and $^{\cdot}NO$ can evolve in cellular systems to H_2O_2 (via dismutation) and nitrite (NO_2^-, via oxidation), respectively, and that MPO can participate in oxidative damage to microorganisms including *T. cruzi* (70, 71), we assessed whether MPO-dependent reactions in the presence of H_2O_2 and NO_2^- (23, 31, 72, 73) could play a role in macrophage-dependent oxidation and cytotoxicity toward *T. cruzi*. First, MPO protein was not detectable in control or LPS plus INF-γ-stimulated J774 macrophages (supplemental Fig. 1). Second, incubation of unstimulated macrophages with relevant levels of NO_2^- to test the contribution of MPO, or even other existing peroxidase activity in macrophages (74), in the generation of oxidizing and nitrating species (31, 72, 75) did not result in either probe oxidation (*i.e.* luminol or DHR) (not shown) or *T. cruzi* protein oxidation/nitration (supplemental Fig. 2). Thus, MPO does not contribute to the formation of oxidant species in *T. cruzi*-infected J774A-1 macrophages.

Intraphagosomal Peroxynitrite in T. cruzi Infection: Microbicidal Activity and Role of Parasite Cytosolic Peroxiredoxin—We examined the integrity of the internalized trypomastigotes in control and iNOS-containing macrophages by transmission electron microscopy at 1 h post-infection (Fig. 5). In unstimulated macrophages, where $O_2^{\cdot-}$ and H_2O_2 are the main oxidant species released to the phagosome during *T. cruzi* internalization, well preserved parasites were observed in the host cell, residing inside phagosomes. Parasite structures such as the nucleus, mitochondrion with kinetoplast, reservosomes, and flagellar pocket were present, and no major morphological alterations were observed (Fig. 5, *upper panel*). On the other hand, internalization in activated macrophages caused marked changes in the parasite ultrastructure, including compact condensation of nuclear and mitochondrial kinetoplast DNA and an intense cytoplasmic vacuolization (Fig. 5, *lower panel*). Moreover, visible disruption of the parasite membrane integrity was observed under this condition (Fig. 5, *arrows*).

To confirm that the cytotoxicity and damage observed in parasites was due to peroxynitrite, macrophages were infected with *T. cruzi* overexpressing *Tc*CPX, an antioxidant enzyme known to detoxify peroxynitrite ($k = 2 \times 10^6\ M^{-1}{\cdot}s^{-1}$) (35, 76). We have recently shown that epimastigotes overexpressing *Tc*CPX are highly resistant to peroxynitrite generated *in vitro* or released to the extracellular medium from activated macrophages (28). First, phagocytosed *Tc*CPX-overexpressing trypomastigotes loaded with DHR fully inhibited INF-γ/LPS-activated macrophages and peroxynitrite-dependent probe oxidation in contrast to wild type parasites. This is in agreement with the enhanced capacity of these genetically modified cells to detoxify peroxynitrite (Fig. 6*A*). Moreover, cytotoxicity studies were carried out in wild type and *Tc*CPX-overexpressing trypomastigotes preloaded with [5,6-^{3}H]uridine, which can be used as a sensitive probe of parasite membrane permeability integrity (77). Macrophages activated with INF-γ and LPS were toxic to wild type trypomastigotes as evaluated by the release of radioactivity to the culture medium supernatant at 2 h of infection, indicative of membrane permeability loss, whereas *Tc*CPX-overexpressing cells showed resistance (Fig. 6*B*), indicating that the simultaneous generation of $O_2^{\cdot-}$ and $^{\cdot}NO$ is involved in the cytotoxic effect of macrophages on internalized parasites at this time point of

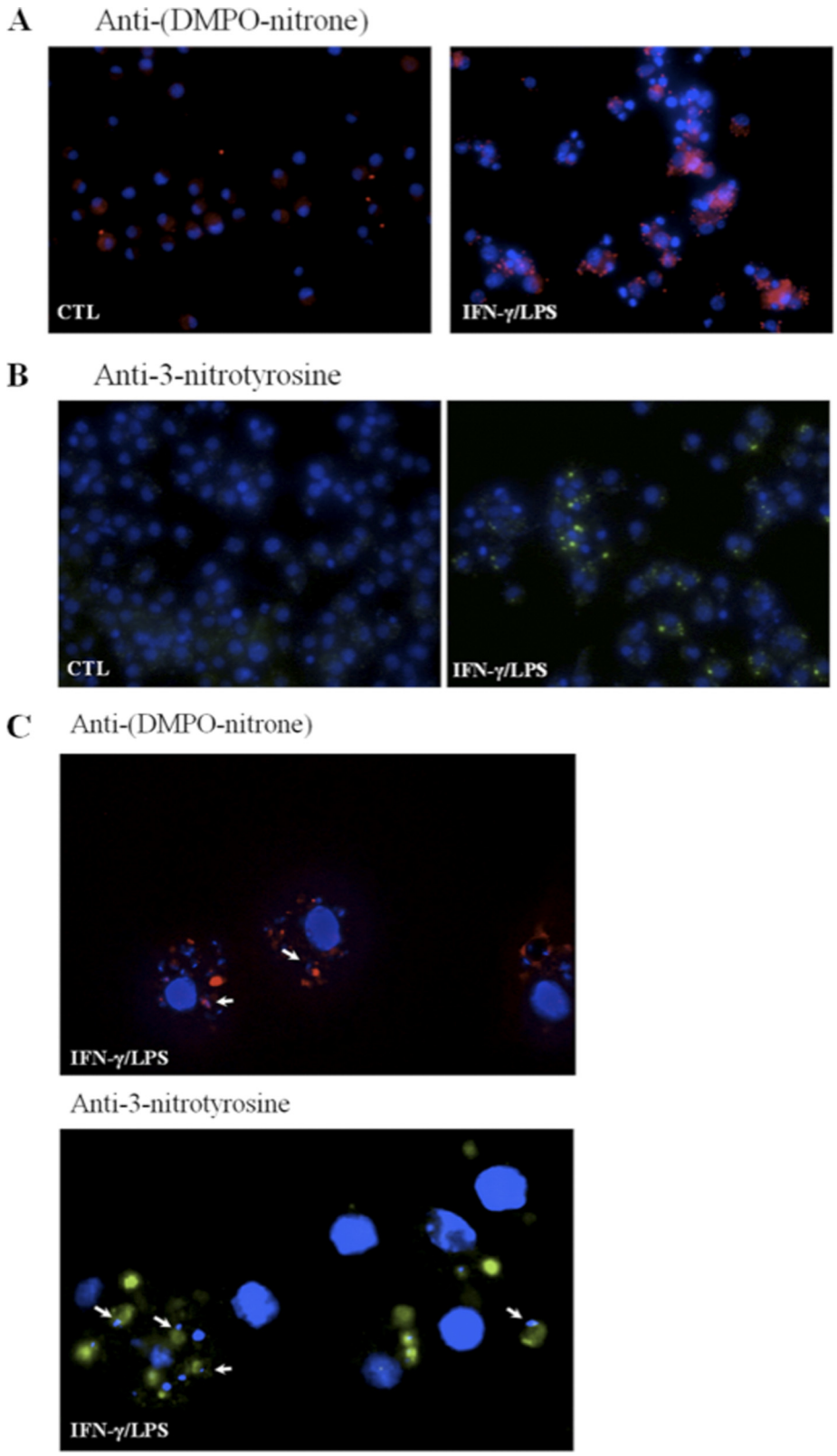

FIGURE 4. **Detection of peroxynitrite-dependent protein oxidation in phagocytosed trypomastigotes.** *A*, DMPO protein adducts. Unstimulated (*CTL*) or activated (*IFN-γ/LPS*) macrophages were infected with DMPO-loaded trypomastigotes (20:1). After 2 h, cells were fixed, permeabilized, incubated with anti-DMPO-nitrone polyclonal antibody, and visualized with Alexa-594-conjugated anti-rabbit antibody. DMPO protein adducts are shown in *red* and nuclei in *blue* (magnification, ×400). *B*, protein 3-nitrotyrosine. Unstimulated or activated macrophages were infected with *T. cruzi* trypomastigotes (20:1). Following phagocytosis (2 h), macrophages were incubated with anti-3-nitrotyrosine antibody and visualized with Alexa-488-conjugated anti-rabbit antibody. 3-Nitrotyrosine staining is shown in *green*, and the nucleus is stained in *blue* (magnification, ×400). *C*, magnified field (×1000) of anti-DMPO-nitrone (*red*) or anti- 3-nitrotyrosine (*green*) in activated macrophages. *Arrows* indicate the distinctive parasite kinetoplast or nuclei revealed by the *blue* DAPI staining in close proximity to the oxidized proteins. Results are representative of at least three independent experiments performed on separate days.

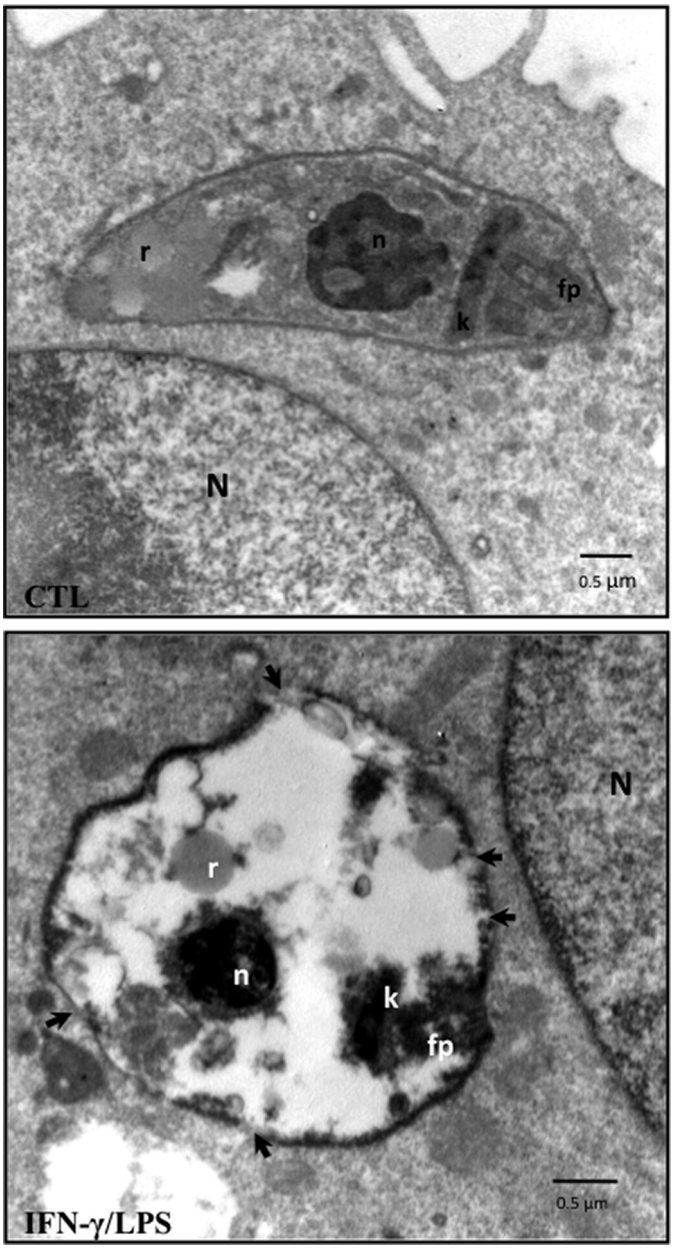

FIGURE 5. **Electron microscopy studies of *T. cruzi* infection.** Micrographs showing unstimulated (*CTL*) and activated (*IFN-γ/LPS*) infected macrophages at 1 h post-infection. The *arrows* in the *lower panel* indicate disruptions of membrane integrity. *N*, macrophage nucleus; *T. cruzi n*, *T. cruzi* nucleus; *k*, kinetoplast; *fp*, flagellar pocket; *r*, reservosomes. The electron micrographs are representative of at least three independent experiments.

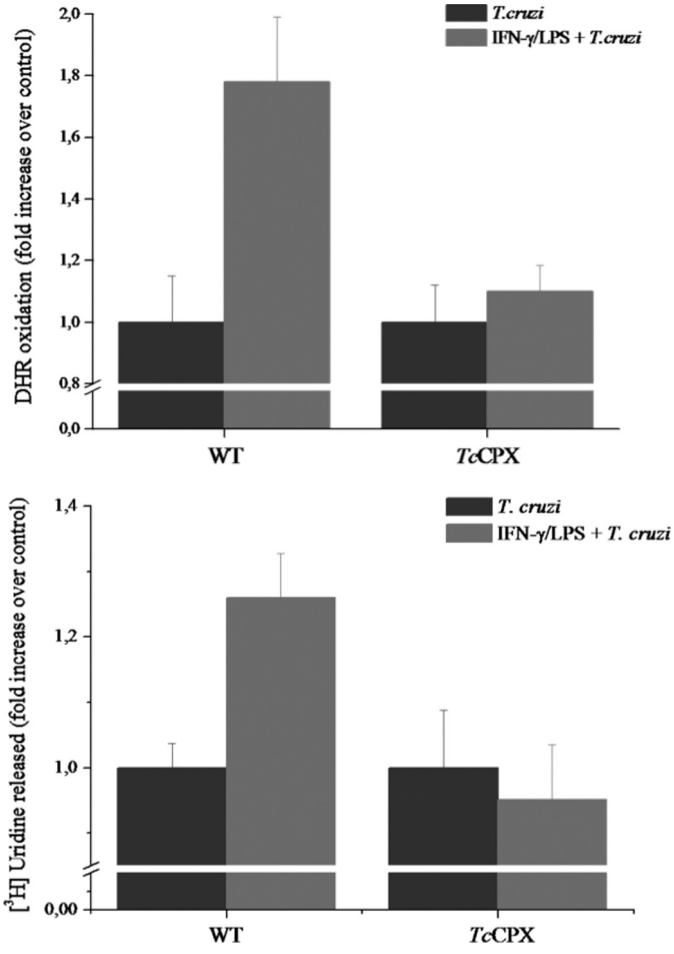

FIGURE 6. ***T. cruzi* killing by intraphagosomal peroxynitrite and protective effect of parasite cytosolic peroxiredoxin.** *A*, wild type (*WT*) or *Tc*CPX-overexpressing trypomastigotes preloaded with DHR were exposed to unstimulated (*T. cruzi*) or activated macrophages (*IFN-γ/LPS* + *T. cruzi*). RH 123 accumulation after 2 h of infection was determined in a fluorescence plate reader. *B*, macrophages were infected with wild type or *Tc*CPX-overexpressing trypomastigotes preloaded with [5,6-^{3}H]uridine. After incubation (for 2 h) supernatants were collected, and radioactivity was measured in a liquid scintillation counter as described under "Experimental Procedures." Data are the mean ± S.E. of three independent experiments.

the infection. *Tc*CPX also reacts fast with $O_2^{\cdot-}$-derived H_2O_2 ($k = 3 \times 10^7\ M^{-1}{\cdot}s^{-1}$) (76) *in vitro*. However, no significant inhibitory effects on probe oxidation or parasite toxicity by *Tc*CPX-overexpressing cells were observed when H_2O_2 from unstimulated macrophages was formed (Figs. 5 and 6). These data fully support H_2O_2 as not being a major effector in macrophage-dependent oxidative reactions in *T. cruzi*, showing that the observed antioxidant and cytoprotective effects of *Tc*CPX are consistent with a prime role on peroxynitrite detoxification, in line with previous observations (28).

The progression of an infection in macrophages was evaluated after 24 h by counting the number of amastigote/100 macrophages (Table 1). Given that the infection process itself triggers $O_2^{\cdot-}$ production, we first performed experiments on unstimulated macrophages in the absence and presence of apocynin to evaluate $O_2^{\cdot-}$- or H_2O_2-mediated cytotoxicity. This inhibitor did not increase the parasite load in unstimulated macrophages, giving further support to our argument that, alone, neither $O_2^{\cdot-}$ nor H_2O_2 contributes significantly to macrophage cytotoxicty. On the other hand, INF-γ- and LPS-activated macrophages significantly decreased the parasite load of wild type parasites by ~60% (based on amastigote count; Fig. 6*B*) whereas *Tc*CPX-overexpressing cells showed a remarkable tolerance. Apocynin did not affect •NO production from activated macrophages (Fig. 2*A*). However, NADPH oxidase inhibition resulted in a reversal of the trypanocidal activity on iNOS-expressing macrophages, consistent with the synergistic action of $O_2^{\cdot-}$ on •NO-mediated cytotoxicity Indeed, to evaluate the independent contribution that these two reactive species make in controlling parasite load, experiments were also performed with iNOS induction *after* infection; this

TABLE 1
Intraphagosomal peroxynitrite controls wild type *T. cruzi* infection

Macrophage treatment		*T. cruzi* amastigotes/100 macrophages[a]	
		Wild type	*Tc*CPX
Unstimulated		37 ± 13	38 ± 19
	+Apocynin	38 ± 12	ND[b]
IFN-γ/LPS-prestimulated[c]		14 ± 3*	36 ± 9
	+Apocynin	33 ± 14	ND[b]
IFN-γ/LPS post-infection[c]		27 ± 8	ND[b]

[a] The load of *T. cruzi* amastigotes in the macrophage culture was evaluated at 24 h after infection with metacyclic trypomastigotes (parasite:macrophage ratio, 5:1). Data are mean ± S.E. of three independent experiments.
[b] Not determined.
[c] IFN-γ/LPS was added to the macrophage culture 5 h before infection (prestimulated) or 30 min after infection (post-infection). Apocynin (50 μM) was used when indicated to avoid NADPH oxidase assembly.
*, $p < 0.01$.

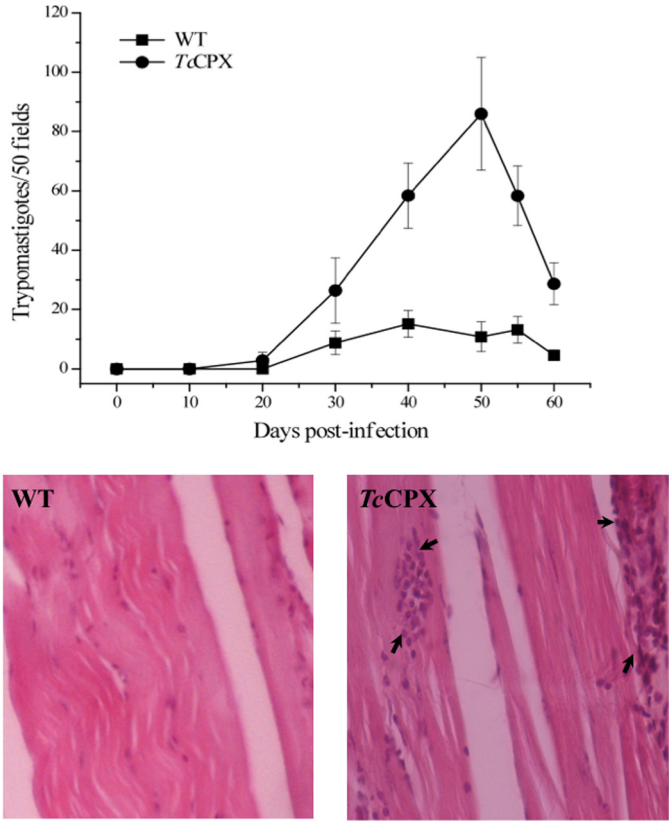

FIGURE 7. **Parasitemia time course and tissue inflammation of mice infected with wild type trypomastigotes or *Tc*CPX overexpressers.** Behavior of wild type (*WT*) and *Tc*CPX-overexpressing-trypomastigotes in experimental mice infections. Two month-old BALB/c mice were infected by intraperitoneal inoculation with 1×10^6 metacyclic trypomastigote forms. Parasitemia and histopathology were analyzed as described under "Experimental Procedures." *A*, parasitemia (trypomastigotes/50 fields) levels elicited by the wild type and *Tc*CPX overexpresser strains. Values are given as means ± S.E. *B*, microphotographs of skeletal muscle tissue sections from mice inoculated with wild type (*left*) and *Tc*CPX overexpressers (*right*) (magnification, ×400). *Arrows* in the *right panel* (*Tc*CPX) indicate inflammatory infiltrates.

circumvented the problem associated with the simultaneous formation of both radicals. Under these conditions, a modest effect on the inhibition of parasite load over the control condition was observed (~30% inhibition on amastigote count), in agreement with a cytostatic role for •NO as described previously (78, 79). Together, the results indicate that the major cytotoxic effect depends on the concomitant production of •NO and $O_2^{\cdot-}$ leading to peroxynitrite formation.

Peroxynitrite Participates in the Control of T. cruzi Infection in Vivo—BALB/c mice were infected by intraperitoneal injection with wild type or the *Tc*CPX overexpressers, metacyclic trypomastigotes. Parasitemia were evaluated every 10 days over a 60-day period, after which the animals were sacrificed and estimations made of tissue damage. Fig. 7*A* shows that the overexpression of *Tc*CPX in trypomastigotes augments virulence as evidenced by a 3-fold increase in parasitemia by day 50. The analysis of heart and skeletal muscle tissue sections showed more prominent inflammatory infiltrates in both tissues in animals infected with the *Tc*CPX overexpressers compared with the wild type trypomastigote-infected group (Fig. 7*B*).

DISCUSSION

During the course of the infection process, macrophages produce reactive oxygen and nitrogen species that are cytotoxic to several microbes including bacteria and parasites (17, 80–82). The production of $O_2^{\cdot-}$ depends on the activation of the NADPH oxidase complex, assembly of which is triggered by receptor-mediated phagocytosis. The precursor of reactive nitrogen species, •NO, is produced after the cytokine-dependent induction of iNOS. This has led to the hypothesis (12, 13, 15, 83) that after microorganisms are ingested, $O_2^{\cdot-}$ formed inside the phagocytic vacuole will react with •NO diffusing from the cytosol to form microbicidal amounts of peroxynitrite. However, direct evidence for this phenomenon at the phagosomal level during microbial infection of macrophages has not been provided.

The importance of oxidant production as the first line of defense of macrophages is underscored by the fact that some pathogens (84), mostly unicellular parasites, have evolved to evade the activation of these sets of enzymes in order to efficiently infect the host. For instance, *Leishmania donovani* promastigotes are internalized by macrophages without eliciting a respiratory burst, thereby avoiding $O_2^{\cdot-}$ production (85), and can also down-regulate macrophage •NO production (86). Additionally, *T. cruzi* as well as other pathogenic trypanosomatids have an ample and well distributed set of antioxidant enzymes to cope with reactive oxygen and nitrogen species (28, 52, 87, 88).

Thus, to test our hypothesis, it was first essential to evaluate the influence of the infective forms of *T. cruzi* on the routes of $O_2^{\cdot-}$ and •NO formation and whether these radicals were formed simultaneously during an infection. In this context, the ability of *T. cruzi* trypomastigotes to trigger NADPH oxidase activity and promote the formation of significant levels of $O_2^{\cdot-}$ was confirmed in infection experiments by three independent methods, namely NBT reduction, luminol oxidation, and cyanide-insensitive oxygen consumption (Fig. 1 and data under "Results"). Macrophage-dependent $O_2^{\cdot-}$ production was responsive to the parasite load and was sustained over a 60–90-min period (Fig. 1*B* and oxygen consumption data under "Results"). Luminol, which equilibrates among intra- and extracellular compartments, and oxygen consumption data reflect overall cellular $O_2^{\cdot-}$ production but do not discriminate the cellular sites (*e.g.* intraphagosomal *versus* extracellu-

lar) of $O_2^{\cdot-}$ release. Thus, to assist in the site-specific detection of $O_2^{\cdot-}$ in the phagosome of infected macrophages, NBT was used as a qualitative probe; the insoluble product from the $O_2^{\cdot-}$-mediated reduction of NBT, formazan, was formed, deposited, and co-localized in the same cellular compartment where the internalized trypomastigotes were located (Fig. 1*A*). In regard to the $^{\cdot}NO$ pathway, non-infective epimastigotes inhibited $^{\cdot}NO$ production released by activated macrophages, as confirmed by evaluating both total NO_2^- accumulation and the time course of $^{\cdot}NO$-dependent oxidation of DAF-2DA; this is consistent with iNOS mRNA levels and protein expression (Fig. 2) and in agreement with previous reports (48, 49). Importantly, this inhibitory effect did not operate for trypomastigotes that did not alter $^{\cdot}NO$ production from macrophages; interestingly, trypomastigotes caused some stimulation of the INF-γ-mediated iNOS induction (Fig. 2). The effect of the infective stage on iNOS expression could be attributed to TOLL-2 receptor (TLR2)- and CD-14-mediated recognition of trypomastigotes, which up-regulate iNOS expression (89–92).

Previous work by our group has provided evidence for the cytotoxic effect of macrophage-derived peroxynitrite to *T. cruzi* in model studies with the non-infective epimastigote stage (13, 14, 34, 93). In this study, we focused on the infective trypomastigote stage and the formation of peroxynitrite inside the phagosome of activated macrophages during parasite internalization. The capacity of peroxynitrite to cause oxidative damage to target cells is limited by its short half-life in the biological milieu and depends on the mean diffusion distance to its molecular targets ($<$10 ms, corresponding to $<$10 μm) (13). Electron microscope studies revealed that the distance between the parasite and the phagosomal membrane is quite small (determined to be ≤10–20 nm) (Fig. 5). Therefore, more than 90% of the peroxynitrite formed in the phagosomal lumen will reach parasite targets even in the presence of CO_2 (13).[4] The previously reported lethal peroxynitrite dose for epimastigotes (13) is probably an underestimation when considering trypomastigotes because of the apparent increase in antioxidant enzymes observed during metacyclogenesis (28, 37, 94). The amount of intraphagosomal peroxynitrite formation was sufficient to kill trypomastigotes, as evidenced by protein nitroxidative modifications (Fig. 4), ultrastructural alterations (Fig. 5), and parasite killing (Table 1). Peroxynitrite stands as a significantly more potent cytotoxin against trypomastigotes than H_2O_2, as revealed by the lack of killing in unstimulated macrophages (Table 1). This is in good agreement with previous determinations with reagent peroxynitrite (13) and H_2O_2 (47), respectively.

Protein oxidative damage in phagocytosed trypomastigotes was detected by immunostaining with anti-DMPO-nitrone and anti 3-nitrotyrosine antibodies; this revealed modified protein in close proximity to *T. cruzi* nuclei and kinetoplasts, which further supports the phagosomal generation of peroxynitrite (Fig. 4). This result is in contrast to that reported during the infection of macrophages by *Salmonella typhimurium.* In this case, the bacteria did not co-localize with protein 3-nitrotyrosine because it interfered with NADPH oxidase activation, thereby preventing $O_2^{\cdot-}$ and peroxynitrite formation in the vesicle (16, 95). Alternative systems to account for *T. cruzi* protein tyrosine nitration, such as MPO-H_2O_2-NO_2^- (23, 31, 72, 74, 75), were not operative due to the lack of MPO in J774A-1 macrophages (supplemental Fig. 1). Peroxidase activity in J774A-1 macrophages may arise from cyclooxygenase-2 induction, but this may be relevant only at 15–20 h post-activation (32), a time frame beyond the experiments reported herein and in full agreement with the lack of oxidative effects on *T. cruzi* upon macrophage incubation with NO_2^- (supplemental Fig. 2).

To further evaluate the role of peroxynitrite toxicity and its relationship to the control of macrophage infection, we used chemically transformed trypomastigotes overexpressing *Tc*CPX as a molecular tool; previous work had shown that this enzyme can efficiently detoxify peroxynitrite in *T. cruzi* (28). Although some data on peroxiredoxin activity toward peroxynitrite in biochemical and cellular systems have been provided (28, 35, 96–98), direct and unambiguous confirmation of its capacity to prevent peroxynitrite-mediated effects during microbial infection to mammalian cells was lacking. We found that RH 123 formation on phagocytosed DHR-loaded wild type trypomastigotes depended on peroxynitrite formation and that the observed fluorescence was confined to the phagosome (Fig. 3). Parasites with elevated levels of *Tc*CPX showed less DHR oxidation, in agreement with the increased ability of cells to decompose peroxynitrite (Fig. 6*A*). Importantly, activated macrophages capable of simultaneously producing $O_2^{\cdot-}$ and $^{\cdot}NO$ during internalization of wild type trypomastigotes limited the progression of the infection, causing a decrease of 60% in parasite load when compared with macrophages producing only $O_2^{\cdot-}$ or $^{\cdot}NO$, or even both, but with a temporal mismatch (Table 1). Ultrastructural analysis of phagocytosed parasites by peroxynitrite producing activated macrophages showed marked damage of cellular organelles and disruption of cell membrane (Fig. 5). *Tc*CPX-overexpressing trypomastigotes resisted cytotoxicity as evaluated by a ^{3}[H]uridine release assay (Fig. 6*B*), which is compatible with an efficient neutralization of peroxynitrite, resulting in higher infection yields at 24 h post-infection (Table 1). In line with this finding, experimental infections of mice with trypomastigotes having higher levels of *Tc*CPX resulted in higher parasitemias and tissue inflammation compared with the infection with wild type parasites (Fig. 7). These observations recapitulated well the previous findings of our group, showing a positive association between the levels of peroxiredoxins in several parasite strains and their degree of virulence (37) The role of $^{\cdot}NO$ in the control of *T. cruzi* infection *in vivo* (99) and the fact that parasite peroxiredoxins do not decompose $^{\cdot}NO$, but rather $^{\cdot}NO$-derived peroxynitrite, fully support the notion that peroxynitrite acts as a cytotoxin *in vivo* and the existence of an interplay between peroxynitrite and peroxiredoxins in influencing the outcome of infection (100).

[4] Given its high concentration in biological fluids (1–2 mM), CO_2 is a key reactant for peroxynitrite ($k = 4.6 \times 10^4$ M^{-1} s^{-1}, 37° C, pH 7.4), limiting its diffusion distance. The product of this reaction is the transient nitrosoperoxocarboxylate adduct that undergoes fast homolysis to $CO_3^{\cdot-}$ and $^{\cdot}NO_2$ in ~35% yields (21).

In summary, the present work demonstrates that peroxynitrite is generated within the phagosome of activated macrophages from the reaction of $O_2^{\cdot-}$, arising from the activation of NADPH oxidase secondary to internalization of the parasite, with $^{\cdot}NO$ diffusing from the cytosol. Peroxynitrite was formed for about 60–90 min and in sufficient amounts to diffuse into the parasite and to cause substantial cytotoxicity, to a much larger extent than that of its precursor radicals and H_2O_2. The effects of peroxynitrite were neutralized by the overexpression of *Tc*CPX in the parasites, which facilitated the development of the infection. The dynamic balance between intraphagosomal oxidant production and the activity of key antioxidant enzymes in the parasite at the onset of the infection critically determined parasite infectivity, providing additional insights for the differences observed on natural *T. cruzi* strains of diverse virulence and pathogenicity in the human disease (37).

Acknowledgments—We thank Dr. Shane R. Wilkinson (School of Biological and Chemical Sciences, Queen Mary University of London, UK) for critical reading of the manuscript and generously providing T. cruzi epimastigotes overexpressing cytosolic TcCPX and Dr. Ronald Mason (NIEHS, National Institutes of Health, Research Triangle Park, NC) for the anti-DMPO-nitrone serum. We are grateful to Dr. Gabriela Casanova (Unidad de Microscopía Electrónica, Facultad de Ciencias, Universidad de la República, Uruguay) for help with transmission electron microscopy studies, Dr. Paola Zago and Dr. Miguel Basombrio (Instituto de Patología Experimental, Facultad de Ciencias de la Salud, UNSa-CONICET, Salta, Argentina) for assistance in the preparation of tissue sections, and Cristina Oviedo (Universidad de la República, Uruguay) for assistance with experimental infections.

REFERENCES

1. Babior, B. M. (1984) *J. Clin. Invest.* **73,** 599–601
2. Groemping, Y., and Rittinger, K. (2005) *Biochem. J.* **386,** 401–416
3. Alvarez, M. N., Trujillo, M., and Radi, R. (2002) *Methods Enzymol.* **359,** 353–366
4. De Groote, M. A., Ochsner, U. A., Shiloh, M. U., Nathan, C., McCord, J. M., Dinauer, M. C., Libby, S. J., Vazquez-Torres, A., Xu, Y., and Fang, F. C. (1997) *Proc. Natl. Acad. Sci. U.S.A.* **94,** 13997–14001
5. Fridovich, I. (1997) *J. Biol. Chem.* **272,** 18515–18517
6. Aliberti, J. C., Cardoso, M. A., Martins, G. A., Gazzinelli, R. T., Vieira, L. Q., and Silva, J. S. (1996) *Infect. Immun.* **64,** 1961–1967
7. Cardillo, F., Voltarelli, J. C., Reed, S. G., and Silva, J. S. (1996) *Infect. Immun.* **64,** 128–134
8. Xie, Q. W., Whisnant, R., and Nathan, C. (1993) *J. Exp. Med.* **177,** 1779–1784
9. Martin, E., Nathan, C., and Xie, Q. W. (1994) *J. Exp. Med.* **180,** 977–984
10. MacMicking, J., Xie, Q. W., and Nathan, C. (1997) *Annu. Rev. Immunol.* **15,** 323–350
11. Ischiropoulos, H., Zhu, L., and Beckman, J. S. (1992) *Arch. Biochem. Biophys.* **298,** 446–451
12. Nathan, C., and Shiloh, M. U. (2000) *Proc. Natl. Acad. Sci. U.S.A.* **97,** 8841–8848
13. Alvarez, M. N., Piacenza, L., Irigoín, F., Peluffo, G., and Radi, R. (2004) *Arch. Biochem. Biophys.* **432,** 222–232
14. Denicola, A., Rubbo, H., Rodríguez, D., and Radi, R. (1993) *Arch. Biochem. Biophys.* **304,** 279–286
15. Evans, T. J., Buttery, L. D., Carpenter, A., Springall, D. R., Polak, J. M., and Cohen, J. (1996) *Proc. Natl. Acad. Sci. U.S.A.* **93,** 9553–9558
16. Vazquez-Torres, A., Jones-Carson, J., Mastroeni, P., Ischiropoulos, H., and Fang, F. C. (2000) *J. Exp. Med.* **192,** 227–236
17. Hickman-Davis, J., Gibbs-Erwin, J., Lindsey, J. R., and Matalon, S. (1999) *Proc. Natl. Acad. Sci. U.S.A.* **96,** 4953–4958
18. Vodovotz, Y., Russell, D., Xie, Q. W., Bogdan, C., and Nathan, C. (1995) *J. Immunol.* **154,** 2914–2925
19. Nauser, T., and Koppenol, W. (2002) *J. Phys. Chem. A* **106,** 4084–4086
20. Radi, R., Peluffo, G., Alvarez, M. N., Naviliat, M., and Cayota, A. (2001) *Free Radic. Biol. Med.* **30,** 463–488
21. Ferrer-Sueta, G., and Radi, R. (2009) *ACS Chem. Biol.* **4,** 161–177
22. Quijano, C., Alvarez, B., Gatti, R. M., Augusto, O., and Radi, R. (1997) *Biochem. J.* **322,** 167–173
23. Radi, R. (2004) *Proc. Natl. Acad. Sci. U.S.A.* **101,** 4003–4008
24. Romero, N., Radi, R., Linares, E., Augusto, O., Detweiler, C. D., Mason, R. P., and Denicola, A. (2003) *J. Biol. Chem.* **278,** 44049–44057
25. Rubbo, H., Radi, R., Trujillo, M., Telleri, R., Kalyanaraman, B., Barnes, S., Kirk, M., and Freeman, B. A. (1994) *J. Biol. Chem.* **269,** 26066–26075
26. Szabó, C. (1996) *Free Radic. Biol. Med.* **21,** 855–869
27. Szabó, C., Ischiropoulos, H., and Radi, R. (2007) *Nat. Rev. Drug Discov.* **6,** 662–680
28. Piacenza, L., Peluffo, G., Alvarez, M. N., Kelly, J. M., Wilkinson, S. R., and Radi, R. (2008) *Biochem. J.* **410,** 359–368
29. Quijano, C., Romero, N., and Radi, R. (2005) *Free Radic. Biol. Med.* **39,** 728–741
30. Eu, J. P., Liu, L., Zeng, M., and Stamler, J. S. (2000) *Biochemistry* **39,** 1040–1047
31. Pfeiffer, S., Lass, A., Schmidt, K., and Mayer, B. (2001) *J. Biol. Chem.* **276,** 34051–34058
32. Palazzolo-Ballance, A. M., Suquet, C., and Hurst, J. K. (2007) *Biochemistry* **46,** 7536–7548
33. Rassi, A., Jr., Rassi, A., and Marin-Neto, J. A. (2010) *Lancet* **375,** 1388–1402
34. Thomson, L., Denicola, A., and Radi, R. (2003) *Arch. Biochem. Biophys.* **412,** 55–64
35. Trujillo, M., Budde, H., Piñeyro, M. D., Stehr, M., Robello, C., Flohé, L., and Radi, R. (2004) *J. Biol. Chem.* **279,** 34175–34182
36. Chen, L., Xie, Q. W., and Nathan, C. (1998) *Mol. Cell* **1,** 795–805
37. Piacenza, L., Zago, M. P., Peluffo, G., Alvarez, M. N., Basombrio, M. A., and Radi, R. (2009) *Int. J. Parasitol.* **39,** 1455–1464
38. Kierszenbaum, F., Knecht, E., Budzko, D. B., and Pizzimenti, M. C. (1974) *J. Immunol.* **112,** 1839–1844
39. Torrico, F., Heremans, H., Rivera, M. T., Van Marck, E., Billiau, A., and Carlier, Y. (1991) *J. Immunol.* **146,** 3626–3632
40. Oliveira, M. A., Santiago, H. C., Lisboa, C. R., Ceravollo, I. P., Trinchieri, G., Gazzinelli, R. T., and Vieira, L. Q. (2000) *Exp. Parasitol.* **95,** 96–105
41. McCabe, R. E., and Mullins, B. T. (1990) *J. Immunol.* **144,** 2384–2388
42. Wirth, J. J., and Kierszenbaum, F. (1982) *J. Immunol.* **129,** 2759–2762
43. Reed, S. G., Nathan, C. F., Pihl, D. L., Rodricks, P., Shanebeck, K., Conlon, P. J., and Grabstein, K. H. (1987) *J. Exp. Med.* **166,** 1734–1746
44. Muñoz-Fernández, M. A., Fernández, M. A., and Fresno, M. (1992) *Immunol. Lett.* **33,** 35–40
45. Roman-Campos, D., Duarte, H. L., Sales, P. A., Jr., Natali, A. J., Ropert, C., Gazzinelli, R. T., and Cruz, J. S. (2009) *Basic Res. Cardiol.* **104,** 238–246
46. Cardoni, R. L., Antunez, M. I., Morales, C., and Nantes, I. R. (1997) *Am. J. Trop. Med. Hyg.* **56,** 329–334
47. Tanaka, Y., Tanowitz, H., and Bloom, B. R. (1983) *Infect. Immun.* **41,** 1322–1331
48. Stempin, C., Giordanengo, L., Gea, S., and Cerbán, F. (2002) *J. Leukoc. Biol.* **72,** 727–734
49. Stempin, C. C., Garrido, V. V., Dulgerian, L. R., and Cerbán, F. M. (2008) *Acta Trop.* **106,** 119–127
50. Bergeron, M., and Olivier, M. (2006) *J. Immunol.* **177,** 6271–6280
51. Piacenza, L., Peluffo, G., and Radi, R. (2001) *Proc. Natl. Acad. Sci. U.S.A.* **98,** 7301–7306
52. Wilkinson, S. R., Temperton, N. J., Mondragon, A., and Kelly, J. M.

(2000) *J. Biol. Chem.* **275,** 8220–8225
53. Contreras, V. T., Salles, J. M., Thomas, N., Morel, C. M., and Goldenberg, S. (1985) *Mol. Biochem. Parasitol.* **16,** 315–327
54. Bonaldo, M. C., Souto-Padron, T., de Souza, W., and Goldenberg, S. (1988) *J. Cell Biol.* **106,** 1349–1358
55. Baehner, R. L., Boxer, L. A., and Davis, J. (1976) *Blood* **48,** 309–313
56. Baxter, M. A., Leslie, R. G., and Reeves, W. G. (1983) *Immunology* **48,** 657–665
57. Hancock, J. T., and Jones, O. T. (1987) *Biochem. J.* **242,** 103–107
58. Granger, D. L., Taintor, R. R., Boockvar, K. S., and Hibbs, J. B., Jr. (1996) *Methods Enzymol.* **268,** 142–151
59. Nakatsubo, N., Kojima, H., Kikuchi, K., Nagoshi, H., Hirata, Y., Maeda, D., Imai, Y., Irimura, T., and Nagano, T. (1998) *FEBS Lett.* **427,** 263–266
60. Roychowdhury, S., Luthe, A., Keilhoff, G., Wolf, G., and Horn, T. F. (2002) *Glia* **38,** 103–114
61. Luo, Y., and Dorf, M. E. (2001) *Curr. Protoc. Immunol.* Chapter 3, Unit 3.20, doi: 10.1002/0471142735.im0320s22
62. Detweiler, C. D., Deterding, L. J., Tomer, K. B., Chignell, C. F., Germolec, D., and Mason, R. P. (2002) *Free Radic. Biol. Med.* **33,** 364–369
63. Brito, C., Naviliat, M., Tiscornia, A. C., Vuillier, F., Gualco, G., Dighiero, G., Radi, R., and Cayota, A. M. (1999) *J. Immunol.* **162,** 3356–3366
64. Zago, M. P., Barrio, A. B., Cardozo, R. M., Duffy, T., Schijman, A. G., and Basombrío, M. A. (2008) *Infect. Immun.* **76,** 443–451
65. Radi, R., Cosgrove, T. P., Beckman, J. S., and Freeman, B. A. (1993) *Biochem. J.* **290,** 51–57
66. Castro, L., Alvarez, M. N., and Radi, R. (1996) *Arch. Biochem. Biophys.* **333,** 179–188
67. James, P. E., Grinberg, O. Y., and Swartz, H. M. (1998) *J. Leukoc. Biol.* **64,** 78–84
68. Wrona, M., Patel, K., and Wardman, P. (2005) *Free Radic. Biol. Med.* **38,** 262–270
69. Cassina, P., Cassina, A., Pehar, M., Castellanos, R., Gandelman, M., de León, A., Robinson, K. M., Mason, R. P., Beckman, J. S., Barbeito, L., and Radi, R. (2008) *J. Neurosci.* **28,** 4115–4122
70. Villalta, F., and Kierszenbaum, F. (1983) *J. Immunol.* **131,** 1504–1510
71. Cardoni, R. L., Rimoldi, M. T., and de Bracco, M. M. (1984) *Cell. Immunol.* **86,** 518–524
72. Eiserich, J. P., Hristova, M., Cross, C. E., Jones, A. D., Freeman, B. A., Halliwell, B., and van der Vliet, A. (1998) *Nature* **391,** 393–397
73. Brennan, M. L., Wu, W., Fu, X., Shen, Z., Song, W., Frost, H., Vadseth, C., Narine, L., Lenkiewicz, E., Borchers, M. T., Lusis, A. J., Lee, J. J., Lee, N. A., Abu-Soud, H. M., Ischiropoulos, H., and Hazen, S. L. (2002) *J. Biol. Chem.* **277,** 17415–17427
74. Cape, J. L., and Hurst, J. K. (2009) *Arch. Biochem. Biophys.* **484,** 190–196
75. Gomez-Mejiba, S. E., Zhai, Z., Gimenez, M. S., Ashby, M. T., Chilakapati, J., Kitchin, K., Mason, R. P., and Ramirez, D. C. (2010) *J. Biol. Chem.* **285,** 20062–20071
76. Piñeyro, M., Arcari, T., Robello, C., Radi, R., and Trujillo, M. (2010) *Arch. Biochem. Biophys.* 10.1016/j.abb.2010.12.014
77. Rimoldi, M. T., Cardoni, R. L., Olabuenaga, S. E., and de Bracco, M. M. (1981) *Immunology* **42,** 521–527
78. Stuehr, D. J., and Nathan, C. F. (1989) *J. Exp. Med.* **169,** 1543–1555
79. Muñoz-Fernández, M. A., Fernández, M. A., and Fresno, M. (1992) *Eur. J. Immunol.* **22,** 301–307
80. Hurst, J. K., and Lymar, S. V. (1997) *Chem. Res. Toxicol.* **10,** 802–810
81. Gookin, J. L., Allen, J., Chiang, S., Duckett, L., and Armstrong, M. U. (2005) *Infect. Immun.* **73,** 3929–3936
82. Vazquez-Torres, A., Jones-Carson, J., and Balish, E. (1996) *Infect. Immun.* **64,** 3127–3133
83. Fang, F. C. (2004) *Nat. Rev. Microbiol.* **2,** 820–832
84. Mohapatra, N. P., Soni, S., Rajaram, M. V., Dang, P. M., Reilly, T. J., El-Benna, J., Clay, C. D., Schlesinger, L. S., and Gunn, J. S. (2010) *J. Immunol.* **184,** 5141–5150
85. Lodge, R., Diallo, T. O., and Descoteaux, A. (2006) *Cell Microbiol.* **8,** 1922–1931
86. Damatta, R. A., Seabra, S. H., Deolindo, P., Arnholdt, A. C., Manhães, L., Goldenberg, S., and de Souza, W. (2007) *FEMS Microbiol. Lett.* **266,** 29–33
87. Irigoín, F., Cibils, L., Comini, M. A., Wilkinson, S. R., Flohé, L., and Radi, R. (2008) *Free Radic. Biol. Med.* **45,** 733–742
88. Krauth-Siegel, R. L., and Comini, M. A. (2008) *Biochim. Biophys. Acta* **1780,** 1236–1248
89. Campos, M. A., Almeida, I. C., Takeuchi, O., Akira, S., Valente, E. P., Procópio, D. O., Travassos, L. R., Smith, J. A., Golenbock, D. T., and Gazzinelli, R. T. (2001) *J. Immunol.* **167,** 416–423
90. Gazzinelli, R. T., and Denkers, E. Y. (2006) *Nat. Rev. Immunol.* **6,** 895–906
91. Guiñazú, N., Pellegrini, A., Carrera-Silva, E. A., Aoki, M. P., Cabanillas, A. M., Gìronés, N., Fresno, M., Cano, R., and Gea, S. (2007) *Int. J. Parasitol.* **37,** 1243–1254
92. Zhang, S., Kim, C. C., Batra, S., McKerrow, J. H., and Loke, P. (2010) *PLoS Negl. Trop. Dis.* **4,** e648
93. Rubbo, H., Denicola, A., and Radi, R. (1994) *Arch. Biochem. Biophys.* **308,** 96–102
94. Atwood, J. A., 3rd, Weatherly, D. B., Minning, T. A., Bundy, B., Cavola, C., Opperdoes, F. R., Orlando, R., and Tarleton, R. L. (2005) *Science* **309,** 473–476
95. Chakravortty, D., Hansen-Wester, I., and Hensel, M. (2002) *J. Exp. Med.* **195,** 1155–1166
96. Bryk, R., Griffin, P., and Nathan, C. (2000) *Nature* **407,** 211–215
97. Barr, S. D., and Gedamu, L. (2003) *J. Biol. Chem.* **278,** 10816–10823
98. Master, S. S., Springer, B., Sander, P., Boettger, E. C., Deretic, V., and Timmins, G. S. (2002) *Microbiology* **148,** 3139–3144
99. Gutierrez, F. R., Mineo, T. W., Pavanelli, W. R., Guedes, P. M., and Silva, J. S. (2009) *Mem. Inst. Oswaldo Cruz* **104,** Suppl. 1, 236–245
100. Piacenza, L., Alvarez, M. N., Peluffo, G., and Radi, R. (2009) *Curr. Opin. Microbiol.* **12,** 415–421